Elastic Stiffness of a Skyrmion Crystal

Y. Nii,[1,*] A. Kikkawa,[1] Y. Taguchi,[1] Y. Tokura,[1,2] and Y. Iwasa[1,2]
[1]RIKEN Center for Emergent Matter Science (CEMS), Wako 351-0198, Japan
[2]Department of Applied Physics and Quantum-Phase Electronics Center (QPEC), University of Tokyo, Tokyo 113-8656, Japan
(Received 22 July 2014; published 30 December 2014)

We observe the elastic stiffness and ultrasonic absorption of a Skyrmion crystal in the chiral-lattice magnet MnSi. The Skyrmion crystal lattice exhibits a stiffness 3 orders of magnitude smaller than that of the atomic lattice of MnSi, being as soft as the flux line lattice in type-II superconductors. The observed anisotropic elastic responses are consistent with the cylindrical shape of the Skyrmion spin texture. Phenomenological analysis reveals that the spin-orbit coupling is responsible for the emergence of anisotropic elasticity in the Skyrmion lattice.

DOI: 10.1103/PhysRevLett.113.267203 PACS numbers: 75.75.-c, 72.55.+s, 75.30.Kz, 75.47.-m

Topologically stable nanoscale magnetic swirling objects called Skyrmions have been found in certain magnets having crystalline chirality [1]. A Skyrmion consists of a nontrivial spin texture characterized by a topological invariant called the Skyrmion number [1,2]. As revealed by several experiments [3–6], these magnetic Skyrmions mostly condense into a form of the closely packed hexagonal lattice. The Skyrmion crystal (SkX) shows a number of intriguing phenomena, such as the topological Hall effect (THE) [7], Skyrmion magnetic resonance [8], and thermally driven ratchet motion [9]. In addition, creation and annihilation of single Skyrmions has been realized by locally injecting a spin-polarized current [10], and these Skyrmions are easily transported by an electric current density of as low as 10^6 A/m^2 [11,12], which is 5 orders of magnitude smaller than that required to induce domain-wall motion in conventional ferromagnets. These peculiar properties have been attracting interest in the field of spintronics because of their potential applications to Skyrmion-based ultradense information memory devices [1,13,14].

In spite of this extensive research on magnetic Skyrmions, experimental methods for exploring Skyrmions are rather limited. This is partly because the physical (or thermodynamic) quantities that characterize Skyrmions are restricted. Amongst measurements of the magnetic, electric, and thermal properties [7,15–17] for characterizing Skyrmions, the most conventional and widely usable approaches are measurements of ac susceptibility [15,16] or the THE [7]. The latter gives a more reliable identification of the SkX than the former because the THE originates from emergent magnetic fields arising from the noncoplanar spin texture or the Skyrmion number of Skyrmions. Although a giant THE arises under pressure [18,19] or chemical substitutions [19], pristine bulk materials of typical SkX systems, such as MnSi [7] and FeGe, show a relatively small THE that is sometimes undetectable. Also, measurement of the THE is not applicable to insulators [20]. Ultrasonic measurements are a possible alternative to these magnetic and electric measurements and offer notable advantages in several respects. First, they allow direct measurement of the elasticity and viscosity of the SkX. Since the SkX is coupled to the crystal lattice *via* pinning, ultrasound can directly shake and deform the SkX, as schematically shown in Fig. 1. Moreover, modulation of Skyrmion spin texture by ultrasound results in a change of free energy via magnetoelastic interaction. Through these couplings, elastic interactions and relaxational motion of the Skyrmion ensemble can be transferred to the ultrasonic waves, leading to additional contributions to the real (stiffness) and imaginary (absorption) parts of the ultrasonic response. Therefore, investigation of the viscoelastic properties of Skyrmions may allow us to detect possible phase transitions among crystal, liquid, and glass phases in terms of Skyrmions [21], analogous to

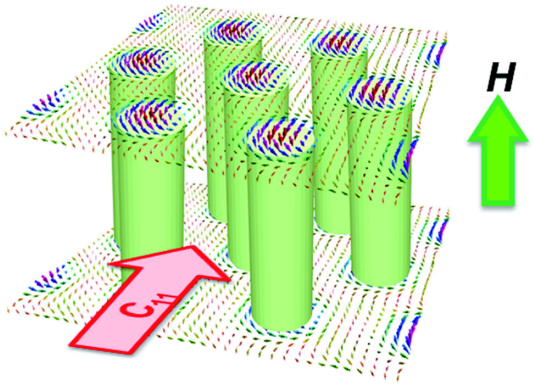

FIG. 1 (color online). Elastic response of Skyrmion crystal to sound wave. In the C_{11} mode, longitudinal ultrasonic waves propagate perpendicularly to the external magnetic field. The inter-Skyrmion distance is directly modulated by the dynamical deformation of the underlying crystal lattice. Thus real (stiffness) and imaginary (absorption) parts of the ultrasonic responses give information on the elastic and viscous behavior of Skyrmion ensembles, respectively.

the flux line lattice (FLL) in type-II superconductors [22,23]. Second, it is possible to unveil the anisotropic properties of the SkX by comparing different elastic modes. Although a cylindrical spin texture of Skyrmions has been directly visualized by electron holography [24], the corresponding anisotropic physical properties remain to be elucidated. Third, the ultrasonic method can be applied to all condensates regardless of their electrical conductivity.

In this Letter, we present ultrasonic measurements of MnSi, as a powerful probe to investigate the elastic and viscous properties of Skyrmions. Pioneering work on the ultrasonic absorption of MnSi was reported in 1976 [25], showing the first identification of the A phase now assigned to the SkX state. The present study reports comprehensive viscoelastic properties of the A phase obtained by detailed measurements of not only ultrasonic absorption but also stiffness. We show the emergence of a distinct elastic stiffness associated with the SkX formation and remarkable ultrasonic absorption in the Skyrmion melting regime. We also found the elastic anisotropy of the SkX, which can be ascribed to spin-orbit coupling (SOC) according to the phenomenological Landau theory.

A single crystal of MnSi was grown by the Czochralski method and was cut into a cuboid shape with the approximate dimensions $4 \times 3 \times 3$ mm^3. The two end surfaces were carefully polished, and 36° Y-cut $LiNbO_3$ piezoelectric transducers were attached on both surfaces with room temperature vulcanizing silicon rubber for the generation and detection of the ultrasound. Ultrasonic studies were carried out by using a conventional pulse-echo technique based on a phase comparison method. A longitudinal sound wave of 18 MHz was employed. Since the corresponding wavelength of approximately 390 μm is much larger than the helical period (18 nm), the induced distortion is regarded as homogeneous for the magnetic system. In the C_{11} mode, the propagation and displacement vectors of the longitudinal ultrasound are along the [100] direction, whereas the external magnetic fields are along the [001] direction; thus the ultrasound modulates the inter-Skyrmion distance. The error estimates and sample dependences of the ultrasonic measurements are described in the Supplemental Material [26]. The ac magnetic susceptibility was simultaneously measured with the use of excitation and pick-up coils covering the sample and transducers. An ac magnetic field with a frequency of 14.626 Hz was applied parallel to the external dc field.

Figures 2(a)–2(c) show the elastic constant C_{11}, the ultrasonic absorption α_{11}, and the magnetic susceptibility Reχ of MnSi, respectively, for discussing the emergent elasticity of the SkX. The three physical properties, which were simultaneously measured, are represented with offsets. At the lowest temperature of 26 K, C_{11} shows a slight decrease up to H_{c1}, followed by a sudden increase at H_{c2}. These critical magnetic fields represent phase transitions from the helical to the conical phases, and then from the

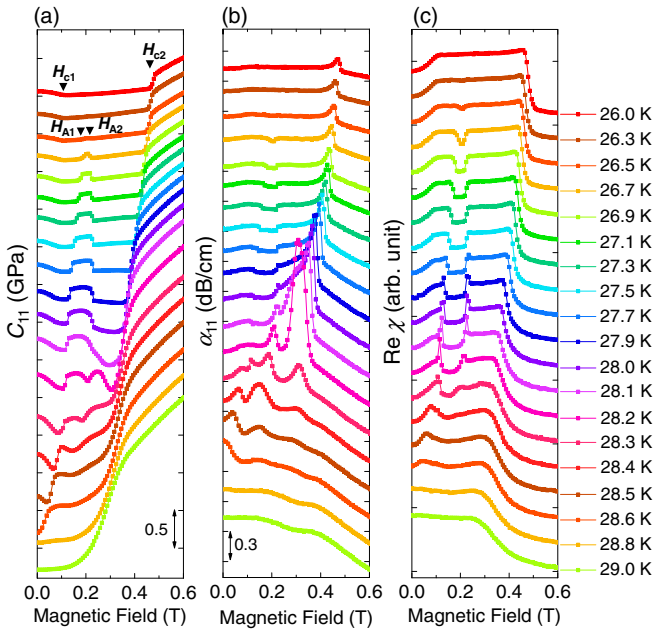

FIG. 2 (color online). Magnetic field dependence of the (a) elastic constant C_{11}, (b) ultrasonic absorption α_{11}, and (c) magnetic susceptibility Reχ at different temperatures. The data are shown with offsets for clarity.

conical to the induced ferromagnetic (IFM) phases, respectively. Above 26.5 K at which a magnetic-field scan cuts across the SkX phase, a distinct elastic harderning appears around 0.2 T between H_{A1} and H_{A2}. This anomaly becomes more pronounced with increasing temperature, and the region between H_{A1} and H_{A2} grows. In the same magnetic field region, Reχ also exhibits a clear depression, as shown in Fig. 2(c), which is characteristic of the SkX phase [15,16]. Therefore, we can conclude that the elastic anomaly between H_{A1} and H_{A2} is of Skyrmion origin. The abrupt elastic hardening associated with the SkX formation is approximately 0.1 GPa. This emergent elasticty is 3 orders of magnitude smaller than the elastic constant of typical inorganic crystals, 1 or 2 orders of magnitude smaller than that of molecular crystals [27], and is comparable to that of the FLL in type-II superconductors [23]. This suggests that the Skyrmion crystal lattice has an extremely *soft* elastic stiffness, as expected from its magnetic origin with much larger periodicity. Near T_c where the SkX begins to melt into the intermediate (IM) phase, the behavior of C_{11} is complex. These elastic anomalies disappear above 28.6 K, above which magnetic-field scans are outside the SkX region.

On the other hand, in the imaginary part of the ultrasonic response α_{11}, a distinguishing feature appears along phase boundaries. At the low-temperature side far below T_c, one can observe a single peak at H_{c2} and a slight depression in the regime of the SkX phase. Approaching T_c, the peak at H_{c2} becomes large and is pronounced at 28.2 K [see also Fig. 2(b)]. The point at which this divergent anomaly takes

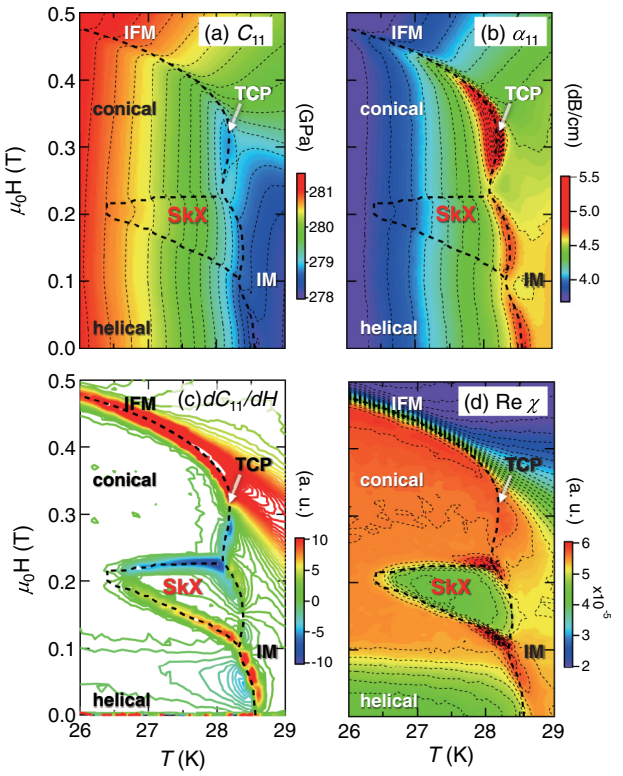

FIG. 3 (color online). Contour maps of the (a) elastic constant C_{11}, (b) ultrasonic absorption α_{11}, (c) magnetic-field derivative of C_{11}, and (d) Reχ. All magnetic ordered phases are characterized in terms of elastic responses. IFM, IM, and TCP stand for induced ferromagnetic phase, intermediate phase, and tricritical point, respectively.

place corresponds to the tricritical point (TCP) [17]. Another large ultrasonic absorption shows up at melting regions of the SkX and the helical phases between 28.3 and 28.6 K. Such prominent features around T_c are absent in the magnetic susceptibility curves [Fig. 2(c)].

Figure 3 shows a summary of the ultrasonic responses in comparison with the magnetic responses by contour mappings in the magnetic phase diagram of MnSi. Figures 3(a) and 3(b) are the contour mappings of C_{11} and α_{11}. (A comparison of these values with previous reports [28,29] is shown in the Supplemental Material [26].) Broad elastic softening and ultrasonic absorption occur in the IM phase, consistent with the previous report at 0 T [28]. Although these broad anomalies are comparatively large, the SkX phase is discernable as kinks in the contour lines. Figure 3(c) is a contour mapping of dC_{11}/dH, which clearly identifies the SkX phase, as well as all other magnetic phases, showing fair agreement with that seen in Reχ [Fig. 3(d)]. This verifies that the SkX and other magnetic phases, such as the conical and the helical phases, can be characterized in terms of elasticity. (As shown in the Supplemental Material [26], the derivatives of the other variables $d\mathrm{Re}\chi/dH$ and $d\alpha_{11}/dH$ can also identify the SkX phases, similarly to the contour mapping of dC_{11}/dH).

As shown in Fig. 3(b), there are three regions in which strong ultrasonic absorption shows up. The largest one appears around the TCP. This can be attributed to the critical spin fluctuation since the slow spin dynamics can attenuate ultrasound via a modulation of exchange coupling [30]. Another one appears just around a region where the SkX melts into the IM phase. Since the phase transition is of first order, the conventional critical spin fluctuation mechanism may be less relevant in this region. Furthermore, the intensity of the ultrasonic absorption is not constant along the phase boundary, but is strong in the temperature region just above the SkX phase. This suggests that the enhanced α_{11} is of Skyrmion origin. As reported by Schulz *et al.* [11], the critical current density to drive the SkX steeply increases with increasing temperature toward T_c. This is reminiscent of the so-called peak effect in the FLL in type-II superconductors [34,35], where the critical current to induce FLL motion steeply increases, showing a peak. Schulz *et al.* explained the steep increase of the critical current, following an FLL scenario: since the elastic energy of the SkX wins over the pinning force at low temperature, the critical current to overcome the pinning forces becomes low. Near T_c, on the other hand, the pinning force begins to win over the elastic energy of the SkX due to the softening of the SkX, and thus the critical current steeply increases. If this is the case, the softening of the SkX near T_c should accompany the relaxational dynamics of the Skyrmion ensemble, which attenuates ultrasound. This is similar to the strong ultrasonic absorption confirmed through the relaxational motion of the FLL in type-II superconductors [23]. Therefore, the ultrasonic absorption distributed in the temperature region immediately above the SkX phase can be understood in terms of the viscous motion of the Skyrmion ensemble. The other large ultrasonic absorption present at the boundary between the helical and the IM phases may also be attributed to a viscous motion of the helical structure since this is also a first-order phase transition.

Figure 4(a) shows the elastic constants C_{11} and C_{33} at 27.5 K. The corresponding elastic strains for C_{11} and C_{33} are schematically illustrated in Figs. 4(c) and 4(d). The C_{33} mode causes a deformation that compresses the crystal and Skyrmion lattices parallel to H, whereas the C_{11} mode causes a deformation that compresses them perpendicular to H. Although these two modes are crystallographically equivalent, the application of magnetic fields breaks the cubic symmetry, allowing a difference between the two. As shown in Fig. 4(a), with increasing H, C_{11} smoothly decreases, whereas C_{33} increases. The difference between C_{11} and C_{33} reaches approximately 0.2 GPa at H_{c1}. Above H_{c1}, both C_{11} and the C_{33} show little H dependence except a sudden change in the regime of the A phase; the C_{11} mode becomes hard, whereas the C_{33} mode becomes soft. These

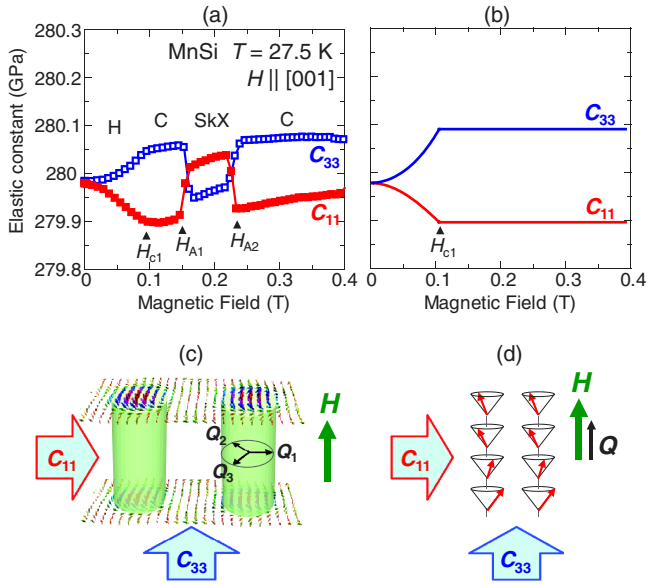

FIG. 4 (color online). Anisotropic elastic response of MnSi. (a), (b) Experiment and theoretical calculation of two different elastic modes of C_{11} and C_{33} as a function of magnetic field at a fixed temperature. H and C stand for the helical and the conical phases, respectively. Schematic illustrations of the two deformation modes with respect to the (c) Skyrmion crystal and (d) conical states. The C_{11} and C_{33} arrows represent the propagation and displacement vector of longitudinal ultrasound.

experimental results clearly reveal that a structure with modulations that have propagation vectors transverse to the field direction (SkX) and the single-Q (conical and helical) states show the opposite character from each other in terms of anisotropy. The SkX is softer in the out-of-plane ($\perp Q$) direction than in the in-plane direction, whereas the helical and the conical structures are softer in the in-plane direction ($\perp Q$) than in the out-of-plane ($\| Q$) direction.

In order to explain the elastic behavior, we calculated the elastic stiffness versus magnetic field for the helical and the conical phases based on the Ginzburg-Landau (GL) phenomenological theory. Here, we assume that strain induced by ultrasound (typically 10^{-7} [30]) does not modify the spin textures with respect to the crystal lattice. This is reasonable in a pinning regime. In this situation, we can treat ultrasound as a perturbative strain, and the elastic response of magnetic origin arises from magnetoelastic coupling. The free energy considered here was originally introduced by Plumer *et al.* in order to reproduce the magnetostriction of MnSi at 4 K [33]. It takes into account the magnetoelastic energy, as well as the magnetic and elastic energies. We applied their method to calculate the elastic constants (see the Supplemental Material for details [26]). Figure 4(b) shows the calculated C_{11} and C_{33} as a function of the magnetic field, showing good agreement with the experimental results for the helical and the conical phases. This analysis revealed that the SOC brings about clear elastic anisotropy among these magnetic phases. Although there is a dominant contribution from exchange interactions, it does not contribute to the elastic anisotropy of the helical and the conical phases.

Finally, we discuss the reversal of the elastic anisotropy in the SkX phase. According to the GL analysis, the effect of SOC on the elasticity leads to the feature that MnSi is hard along the Q vector and soft perpendicular to the Q vector. This is because the coefficient of the magnetoelastic term originating from SOC in the GL free energy is positive [see L_1 and L_2 in Eq. (3) in the Supplemental Material [26]]. In the conical phases, the Q vector is parallel to $H\|$ [001]. Thus, the conical state is hard along [001] and is soft perpendicular to [001], meaning that $C_{11} < C_{33}$. In the SkX phase, on the other hand, the Q vectors of three helices are perpendicular to H. Thus, the SkX is hard perpendicular to [001] and soft along [001], meaning that $C_{11} > C_{33}$. The relatively small anisotropy of the SkX is understood by considering that the elastic anisotropies stemming from three helices average out each of the anisotropy behaviors. Incidentally, in the helical state at $H = 0$, the elastic anisotropy is smeared out, as observed [Fig. 4(a)], since four equivalent helical domains with $Q\|\langle 111\rangle$ are present. Application of a magnetic field continuously induces elastic anisotropy through the gradual rotation of the Q vector in the H direction.

To summarize, we revealed that the SkX is an anisotropic elastic object, which has a stiffness 3 orders of magnitude smaller than that of the host lattice, being as soft as the FLL in type-II superconductors. The observed anisotropic stiffness was qualitatively understood by the SOC. These results are suggestive of several new directions of Skyrmion manipulation, for instance, by the application of local stress through anisotropic strain, as theoretically discussed by Butenko *et al.* [36].

We are grateful to T. Arima and X. Z. Yu for enlightening discussions. This work is supported by JSPS through the Funding Program for World-Leading Innovative R&D on Science and Technology (FIRST program), and Grant-in-Aids for Scientific Research (S) (Grant No. 24224009) and for Specially Promoted Research (Grant No. 25000003). Y. N. was supported by an Incentive Research Grant from RIKEN.

*yoichi.nii@riken.jp

[1] N. Nagaosa and Y. Tokura, Nat. Nanotechnol. **8**, 899 (2013).
[2] B. Binz and A. Vishwanath, Physica (Amsterdam) **403B**, 1336 (2008).
[3] S. Mühlbauer, B. Binz, F. Jonietz, C. Pfleiderer, A. Rosch, A. Neubauer, R. Georgii, and P. Böni, Science **323**, 915 (2009).
[4] X. Z. Yu, Y. Onose, N. Kanazawa, J. H. Park, J. H. Han, Y. Matsui, N. Nagaosa, and Y. Tokura, Nature (London) **465**, 901 (2010).

[5] S. Heinze, K. Bergmann, M. Menzel, J. Brede, A. Kubetzka, R. Wiesendanger, G. Bihlmayer, and S. Blügel, Nat. Phys. **7**, 713 (2011).
[6] P. Milde, D. Köhler, J. Seidel, L. M. Eng, A. Bauer, A. Chacon, J. Kindervater, S. Mühlbauer, C. Pfleiderer, S. Buhrandt, C. Schütte, and A. Rosch, Science **340**, 1076 (2013).
[7] A. Neubauer, C. Pfleiderer, B. Binz, A. Rosch, R. Ritz, P. G. Niklowitz, and P. Böni, Phys. Rev. Lett. **102**, 186602 (2009).
[8] Y. Onose, Y. Okamura, S. Seki, S. Ishiwata, and Y. Tokura, Phys. Rev. Lett. **109**, 037603 (2012).
[9] M. Mochizuki, X. Z. Yu, S. Seki, N. Kanazawa, W. Koshibae, J. Zang, M. Mostovoy, Y. Tokura, and N. Nagaosa, Nat. Mater. **13**, 241 (2014).
[10] N. Romming, C. Hanneken, M. Menzel, J. E. Bickel, B. Wolter, K. Bergmann, A. Kubetzka, and R. Wiesendanger, Science **341**, 636 (2013).
[11] T. Schulz, R. Ritz, A. Bauer, M. Halder, M. Wagner, C. Franz, C. Pfleiderer, K. Everschor, M. Garst, and A. Rosch, Nat. Phys. **8**, 301 (2012).
[12] X. Z. Yu, N. Kanazawa, W. Z. Zhang, T. Nagai, T. Hara, K. Kimoto, Y. Matsui, Y. Onose, and Y. Tokura, Nat. Commun. **3**, 988 (2012).
[13] A. Fert, V. Cros, and J. Sampairo, Nat. Nanotechnol. **8**, 152 (2013).
[14] J. Sampairo, V. Cros, S. Rohart, A. Thiaville, and A. Fert, Nat. Nanotechnol. **8**, 839 (2013).
[15] H. Wilhelm, M. Baenitz, M. Schmidt, U. K. Röler, A. A. Leonov, and A. N. Bogdanov, Phys. Rev. Lett. **107**, 127203 (2011).
[16] A. Bauer and C. Pfleiderer, Phys. Rev. B **85**, 214418 (2012).
[17] A. Bauer, M. Garst, and C. Pfleiderer, Phys. Rev. Lett. **110**, 177207 (2013).
[18] R. Ritz, M. Halder, C. Franz, A. Bauer, M. Wagner, R. Bamler, A. Rosch, and C. Pfleiderer, Phys. Rev. B **87**, 134424 (2013).
[19] B. J. Chapman, M. G. Grossnickle, T. Wolf, and M. Lee, Phys. Rev. B **88**, 214406 (2013).
[20] S. Seki, X. Z. Yu, S. Ishiwata, and Y. Tokura, Science **336**, 198 (2012).
[21] U. K. Röler, A. N. Bogdanov, and C. Pfleiderer, Nature (London) **442**, 797 (2006).
[22] G. Blatter, M. V. Feigel'man, V. B. Geshkenbein, A. I. Larkin, and V. M. Vinokur, Rev. Mod. Phys. **66**, 1125 (1994).
[23] J. Pankert, G. Marbach, A. Comberg, P. Lemmens, P. Fröning, and S. Ewert, Phys. Rev. Lett. **65**, 3052 (1990).
[24] H. Park, X. Yu, S. Aizawa, T. Tanigaki, T. Akashi, Y. Takahashi, T. Matsuda, N. Kanazawa, Y. Onose, D. Shindo, A. Tonomura, and Y. Tokura, Nat. Nanotechnol. **9**, 337 (2014).
[25] S. Kusaka, K. Yamamoto, T. Komatsubara, and Y. Ishikawa, Solid State Commun. **20**, 925 (1976).
[26] See Supplemental Material at http://link.aps.org/supplemental/10.1103/PhysRevLett.113.267203, which includes Refs. [28–33], for details of the Ginzburg-Landau analysis and ultrasonic measurements.
[27] D. Tahk, H. Lee, and D. Khang, Macromolecules **42**, 7079 (2009).
[28] A. E. Petrova and S. M. Stishov, J. Phys. Condens. Matter **21**, 196001 (2009).
[29] G. P. Zinoveva, L. P. Andreeva, and P. V. Geld, Phys. Status Solidi A **23**, 711 (1974).
[30] B. Lüthi, *Physical Acoustics in the Solid State* (Springer, New York, 2005).
[31] C. Pantea, D. Rickel, A. Migliori, R. Leisure, J. Zhang, Y. Zhao, S. El-Khatib, and B. Li, Rev. Sci. Instrum. **76**, 114902 (2005).
[32] D. I. Bolef and M. Menes, J. Appl. Phys. **31**, 1010 (1960).
[33] M. L. Plumer and M. B. Walker, J. Phys. C **15**, 7181 (1982).
[34] J. Shi, X. S. Ling, R. Liang, D. A. Bonn, and W. N. Hardy, Phys. Rev. B **60**, R12593 (1999).
[35] A. I. Larkin and Y. N. Ovchinnikov, J. Low Temp. Phys. **34**, 409 (1979).
[36] A. B. Butenko, A. A. Leonov, U. K. Röler, and A. N. Bogdanov, Phys. Rev. B **82**, 052403 (2010).